

Mode characteristics of nested eccentric waveguides constructed by two cylindrical nanowires coated with graphene

Ji Liu(刘吉), Lixia Yu(于丽霞), and Wenrui Xue(薛文瑞)

Citation: Chin. Phys. B, 2022, 31 (**3**): 036803. DOI: 10.1088/1674-1056/ac1e17
Journal homepage: http://cpb.iphy.ac.cn; http://iopscience.iop.org/cpb

What follows is a list of articles you may be interested in

NBN-doped nanographene embedded with five- and seven-membered rings on Au(111) surface

Huan Yang(杨欢), Yun Cao(曹云), Yixuan Gao(高艺璇), Yubin Fu(付钰彬), Li Huang(黄立), Junzhi Liu(刘俊治), Xinliang Feng(冯新亮), Shixuan Du(杜世萱), and Hong-Jun Gao(高鸿钧)

Chin. Phys. B, 2021, 30 (**5**): 056802. DOI: 10.1088/1674-1056/abeede

First principles study of behavior of helium at Fe(110)-graphene interface

Yan-Mei Jing(荆艳梅) and Shao-Song Huang(黄绍松)

Chin. Phys. B, 2021, 30 (**4**): 046802. DOI: 10.1088/1674-1056/abd46d

Super-strong interactions between multivalent anions and graphene

Xing Liu(刘星) and Guosheng Shi(石国升)

Chin. Phys. B, 2021, 30 (**4**): 046801. DOI: 10.1088/1674-1056/abd396

Interfaces between MoO_x and MoX_2 (X = S, Se, and Te)

Fengming Chen(陈凤鸣), Jinxin Liu(刘金鑫), Xiaoming Zheng(郑晓明), Longhui Liu(刘龙慧), Haipeng Xie(谢海鹏), Fei Song(宋飞), Yongli Gao(高永立), and Han Huang(黄寒)

Chin. Phys. B, 2020, 29 (**11**): 116802. DOI: 10.1088/1674-1056/abb310

Triphenylene adsorption on Cu(111) and relevant graphene self-assembly

Qiao-Yue Chen(陈乔悦), Jun-Jie Song(宋俊杰), Liwei Jing(井立威), Kaikai Huang(黄凯凯), Pimo He(何丕模), Hanjie Zhang(张寒洁)

Chin. Phys. B, 2020, 29 (**2**): 026801. DOI: 10.1088/1674-1056/ab6583

Mode characteristics of nested eccentric waveguides constructed by two cylindrical nanowires coated with graphene

Ji Liu(刘吉)[1,†], Lixia Yu(于丽霞)[2], and Wenrui Xue(薛文瑞)[3]

[1] *Key Laboratory of Instrumentation Science and Dynamic Measurement of Ministry of Education, North University of China, Taiyuan* 030051, *China*
[2] *School of Information and Communication Engineering, North University of China, Taiyuan* 030051, *China*
[3] *College of Physics and Electronic Engineering, Shanxi University, Taiyuan* 030006, *China*

(Received 11 June 2021; revised manuscript received 22 July 2021; accepted manuscript online 17 August 2021)

A kind of nested eccentric waveguide constructed with two cylindrical nanowires coated with graphene was designed. The mode characteristics of this waveguide were studied using the multipole method. It was found that the three lowest modes (mode 0, mode 1 and mode 2) can be combined by the zero-order mode or/and the first-order modes of two single nanowires. Mode 0 has a higher figure of merit and the best performance among these modes within the parameter range of interest. The mode characteristics can be adjusted by changing the parameters of the waveguide. For example, the propagation length will be increased when the operating wavelength, the minimum spacing between the inner and outer cylinders, the inner cylinder radius and the Fermi energy are increased. However, when the outer cylinder radius, the dielectric constants of region I, or the dielectric constants of region III are increased, the opposite effect can be seen. These results are consistent with the results obtained using the finite element method (FEM). The waveguide structure designed in this paper is easy to fabricate and can be applied to the field of micro/nano sensing.

Keywords: graphene, nanowire, waveguide, multipole method

PACS: 68.65.Pq, 81.07.Gf, 42.81.Qb, 02.30.Mv **DOI:** 10.1088/1674-1056/ac1e17

1. Introduction

Surface plasmon waveguides (SPWs) are a new type of waveguide, which uses surface plasmon polaritons (SPPs)[1] to guide the transmission of electromagnetic waves. The main materials used in SPWs are noble metals,[2] semiconductors,[3] graphene,[4] etc. The size of these waveguides is in micron or nanometer scale, and they are expected to be widely used in highly integrated photonic chips[5] and in the field of sensing.[6] Graphene is a new type of two-dimensional material, which has been applied in many fields.[7–9] Compared to conventional metal materials (e.g., silver and gold), graphene has desirable properties, such as tunability, extreme confinement, crystallinity and low loss. Because of these unique properties, graphene has been recently proposed as a platform for plasmon waveguiding from THz to infrared frequencies.[10] By coating single[11,12] or multi-layer[13–15] graphene on the surface of dielectrics, strip,[16–18] circular,[11,12] elliptical[19] and hybrid[20–26] SPWs can be formed. On this basis, parallel SPWs can be constructed.[27–29]

The nested surface plasmon waveguide coated with graphene is a research hotspot. In 2015, Yang *et al.* designed a circular dielectric nanowire waveguide coated with two layers of graphene,[13] which can be regarded as a coaxial waveguide formed by embedding one graphene-coated dielectric nanowire into the axis of the other. By solving the dispersion equation, it is found that the Fermi energy of graphene, the distance between the two layers of graphene and the radius of the waveguide can affect the behavior of the modes supported by the waveguide. The nested surface plasmon waveguide designed by Liu *et al.* in 2017 can be regarded as a coaxial waveguide formed by embedding a graphene-coated cylindrical silicon nanowire into the axis of another graphene-coated cylindrical silicon dioxide nanowire.[14] The results show that the fundamental mode supported by the waveguide has a longer propagation distance and a smaller mode area. In 2017, Xing *et al.* designed a circular dielectric nanowire waveguide coated with multilayer graphene,[15] which can be regarded as a coaxial waveguide formed by embedding multiple graphene-coated dielectric nanowires with a gradually decreasing radius into the axis of graphene-coated dielectric nanowires with a larger radius. The results show that the waveguide has a strong ability to confine the field, and the mode characteristics can be adjusted by the chemical potential of graphene. In 2019, Cheng *et al.* designed a graphene coated confocal elliptical dielectric nanowire waveguide,[19] which can be regarded as a waveguide formed by embedding one elliptical dielectric nanowire into another and keeping the two elliptical dielectric nanowires confocal. The results show that, compared with the elliptical dielectric nanowire waveguide coated with single-layer graphene, this kind of waveguide has better mode performance and a wider adjustable range. Since a common feature of the above waveguides is that the embedded waveguide and parent waveguide have the same

[†]Corresponding author. E-mail: liuji6@nuc.edu.cn

© 2022 Chinese Physical Society and IOP Publishing Ltd

axis of symmetry, the components of the field can be expanded in the same coordinate system when studying the mode characteristics. Based on the boundary conditions, the dispersion equation is obtained, and then the effective refractive index and field distribution are obtained. If the embedded waveguide is eccentric, this method will not work and the mode characteristics of the waveguide will not be obtained.

In this paper, the mode characteristics of a kind of graphene-coated cylindrical dielectric nanowire waveguide embedded with eccentric cylindrical dielectric nanowire are studied using the multipole method.[30] This method can effectively overcome the difficulties mentioned above. To verify the obtained results, the FEM method is used. This paper is structured as follows. Section 2 gives the theoretical model. Section 3 presents the result and discussion. The last section is the conclusion.

2. Theoretical model

The waveguide structure designed in this paper is shown in Fig. 1. It consists of a circular parent dielectric nanowire (wire 2) with a radius of ρ_{20} and a circular embedded dielectric nanowire (wire 1) with a radius of ρ_{10}. Wire 1 and wire 2 are eccentric. The minimum spacing between the outer surface of wire 1 and the inner surface of wire 2 is s. Suppose that the dielectric constant of wire 1 is ε_1 (region I), wire 2 is ε_2 (region II) and the background is ε_3 (region III). The surface of wire 1 and wire 2 is coated with a single layer of graphene. The conductivity of graphene, σ_g, has been computed within the random-phase approximation.[31] This kind of waveguide structure may be successfully fabricated using the preform-drawing method[32] and chemical vapor deposition (CVD) method.[33]

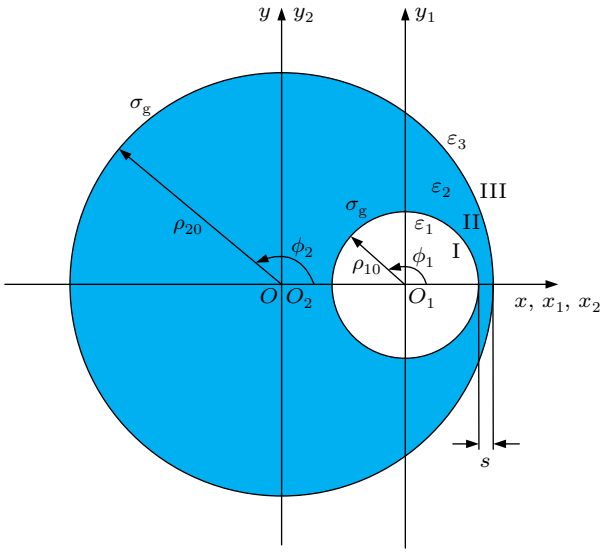


Fig. 1. Crosssection of the waveguide composed of one circular parent dielectric nanowire coated with graphene and one circular embedded dielectric nanowire coated with graphene.

As shown in Fig. 1, the rectangular coordinate system o_1-$x_1y_1z_1$ and the cylindrical coordinate system o_1-$\rho_1\phi_1z_1$ are established with the symmetrical center of wire 1 as the coordinate origin. The rectangular coordinate system o_2-$x_2y_2z_2$, o-xyz and the cylindrical coordinate system o_2-$\rho_2\phi_2z_2$ are established with the symmetrical center of wire 2 as the coordinate origin. According to the multipole method,[30] assuming that wire 1 and wire 2 exist separately, the E_z and H_z fields inside and outside the wire are distributed as follows in their respective coordinate systems:

Inside wire 1:

$$E_{z11}(\rho_1,\phi_1) = \sum_{m=0}^{\infty} A_m I_m(\lambda_{11}\rho_1)\cos(m\phi_1) + \sum_{m=1}^{\infty} A'_m I_m(\lambda_{11}\rho_1)\sin(m\phi_1), \quad (1)$$

$$H_{z11}(\rho_1,\phi_1) = \sum_{m=0}^{\infty} B_m I_m(\lambda_{11}\rho_1)\cos(m\phi_1) + \sum_{m=1}^{\infty} B'_m I_m(\lambda_{11}\rho_1)\sin(m\phi_1). \quad (2)$$

Outside wire 1:

$$E_{z12}(\rho_1,\phi_1) = \sum_{m=0}^{\infty} C_m K_m(\lambda_{12}\rho_1)\cos(m\phi_1) + \sum_{m=1}^{\infty} C'_m K_m(\lambda_{12}\rho_1)\sin(m\phi_1), \quad (3)$$

$$H_{z12}(\rho_1,\phi_1) = \sum_{m=0}^{\infty} D_m K_m(\lambda_{12}\rho_1)\cos(m\phi_1) + \sum_{m=1}^{\infty} D'_m K_m(\lambda_{12}\rho_1)\sin(m\phi_1). \quad (4)$$

Inside wire 2:

$$E_{z21}(\rho_2,\phi_2) = \sum_{m=0}^{\infty} E_m I_m(\lambda_{21}\rho_2)\cos(m\phi_2) + \sum_{m=1}^{\infty} E'_m I_m(\lambda_{21}\rho_2)\sin(m\phi_2), \quad (5)$$

$$H_{z21}(\rho_2,\phi_2) = \sum_{m=0}^{\infty} F_m I_m(\lambda_{21}\rho_2)\cos(m\phi_2) + \sum_{m=1}^{\infty} F'_m I_m(\lambda_{21}\rho_2)\sin(m\phi_2). \quad (6)$$

Outside wire 2:

$$E_{z22}(\rho_2,\phi_2) = \sum_{m=0}^{\infty} G_m K_m(\lambda_{22}\rho_2)\cos(m\phi_2) + \sum_{m=1}^{\infty} G'_m K_m(\lambda_{22}\rho_2)\sin(m\phi_2), \quad (7)$$

$$H_{z22}(\rho_2,\phi_2) = \sum_{m=0}^{\infty} H_m K_m(\lambda_{22}\rho_2)\cos(m\phi_2) + \sum_{m=1}^{\infty} H'_m K_m(\lambda_{22}\rho_2)\sin(m\phi_2). \quad (8)$$

Here, I_m and K_m are m-order Bessel functions, A_m, A'_m, B_m, B'_m, C_m, C'_m, D_m, D'_m, E_m, E'_m, F_m, F'_m, G_m, G'_m, H_m, and H'_m are undetermined coefficients of order m, $\lambda_{11} = \sqrt{\beta^2 - \omega^2\varepsilon_1\varepsilon_0\mu_0}$, $\lambda_{12} = \sqrt{\beta^2 - \omega^2\varepsilon_2\varepsilon_0\mu_0}$, $\lambda_{21} = \sqrt{\beta^2 - \omega^2\varepsilon_2\varepsilon_0\mu_0}$, $\lambda_{22} = \sqrt{\beta^2 - \omega^2\varepsilon_3\varepsilon_0\mu_0}$.

Based on the principle of field superposition, the distributions of E_z and H_z fields in regions I, II, and III are as follows:

$$(E_z)_{\rm I} = E_{z11}(\rho_1,\phi_1) + E_{z21}(\rho_2,\phi_2), \tag{9}$$
$$(H_z)_{\rm I} = H_{z11}(\rho_1,\phi_1) + H_{z21}(\rho_2,\phi_2), \tag{10}$$
$$(E_z)_{\rm II} = E_{z12}(\rho_1,\phi_1) + E_{z21}(\rho_2,\phi_2), \tag{11}$$
$$(H_z)_{\rm II} = H_{z12}(\rho_1,\phi_1) + H_{z21}(\rho_2,\phi_2), \tag{12}$$
$$(E_z)_{\rm III} = E_{z22}(\rho_2,\phi_2) + E_{z12}(\rho_1,\phi_1), \tag{13}$$
$$(H_z)_{\rm III} = H_{z22}(\rho_2,\phi_2) + H_{z12}(\rho_1,\phi_1). \tag{14}$$

Based on the relationship between the transverse component and longitudinal component of the fields,[34] the distribution of transverse fields $(E_\phi)_{\rm I}$, $(H_\phi)_{\rm I}$, $(E_\phi)_{\rm II}$, $(H_\phi)_{\rm II}$, $(E_\phi)_{\rm III}$ and $(H_\phi)_{\rm III}$ in regions I, II and III can be obtained. For example,

$$\begin{aligned}(E_\phi)_{\rm I} = & -\frac{1}{\lambda_{11}^2}\left\{\left(-\frac{{\rm j}\beta}{\rho_1}\right)\left[-\sum_{m=0}^{\infty} mA_m I_m(\lambda_{11}\rho_1)\sin(m\phi_1)\right.\right.\\ & +\sum_{m=1}^{\infty} mA'_m I_m(\lambda_{11}\rho_1)\cos(m\phi_1)\\ & +\frac{\partial}{\partial\phi_1}\left[\sum_{m=0}^{\infty} E_m I_m(\lambda_{21}\rho_2)\cos(m\phi_2)\right.\\ & \left.\left.+\sum_{m=1}^{\infty} E'_m I_m(\lambda_{21}\rho_2)\sin(m\phi_2)\right]\right]\\ & +({\rm j}\omega\mu_0)\left[\sum_{m=0}^{\infty}\lambda_{11}B_m I'_m(\lambda_{11}\rho_1)\cos(m\phi_1)\right.\\ & +\sum_{m=1}^{\infty}\lambda_{11}B'_m I'_m(\lambda_{11}\rho_1)\sin(m\phi_1)\\ & +\frac{\partial}{\partial\rho_1}\left[\sum_{m=0}^{\infty} F_m I_m(\lambda_{21}\rho_2)\cos(m\phi_2)\right.\\ & \left.\left.\left.+\sum_{m=1}^{\infty} F'_m I_m(\lambda_{21}\rho_2)\sin(m\phi_2)\right]\right]\right\}.\end{aligned} \tag{15}$$

This is different to Graf's addition theory used in reference,[30] and the derivative involved in the above formula can be obtained using the following formula:[35,36]

$$\frac{\partial\psi(\rho_2,\phi_2)}{\partial\rho_1} = \frac{\partial\psi(\rho_2,\phi_2)}{\partial\rho_2}\hat{\rho}_2\cdot\hat{\rho}_1 + \frac{\partial\psi(\rho_2,\phi_2)}{\rho_2\partial\phi_2}\hat{\phi}_2\cdot\hat{\rho}_1, \tag{16}$$
$$\frac{\partial\psi(\rho_2,\phi_2)}{\rho_1\partial\phi_1} = \frac{\partial\psi(\rho_2,\phi_2)}{\partial\rho_2}\hat{\rho}_2\cdot\hat{\phi}_1 + \frac{\partial\psi(\rho_2,\phi_2)}{\rho_2\partial\phi_2}\hat{\phi}_2\cdot\hat{\phi}_1. \tag{17}$$

Here, $\hat{\rho}_1$ and $\hat{\phi}_1$ are the transverse unit vectors of coordinates in the cylindrical coordinate system o–$\rho_1\phi_1 z_1$, $\hat{\rho}_2$, and $\hat{\phi}_2$ are the transverse unit vectors of coordinates in the cylindrical coordinate system o–$\rho_2\phi_2 z_2$.

Graphene is regarded as a material with zero thickness and conductivity $\sigma_{\rm g}$. At the interface of regions I, II and III, the following relation of the boundary value of tangential fields can be applied:

$$(E_z)_{\rm I}|_{\rho_1=\rho_{10}} = (E_z)_{\rm II}|_{\rho_1=\rho_{10}}, \tag{18}$$
$$(E_z)_{\rm II}|_{\rho_2=\rho_{20}} = (E_z)_{\rm III}|_{\rho_2=\rho_{20}}, \tag{19}$$
$$(E_\phi)_{\rm I}|_{\rho_1=\rho_{10}} = (E_\phi)_{\rm II}|_{\rho_1=\rho_{10}}, \tag{20}$$
$$(E_\phi)_{\rm II}|_{\rho_2=\rho_{20}} = (E_\phi)_{\rm III}|_{\rho_2=\rho_{20}}, \tag{21}$$
$$(H_z)_{\rm I}|_{\rho_1=\rho_{10}} - (H_z)_{\rm II}|_{\rho_1=\rho_{10}} = \sigma_{\rm g}(E_\phi)_{\rm I}|_{\rho_1=\rho_{10}}, \tag{22}$$
$$(H_z)_{\rm II}|_{\rho_2=\rho_{20}} - (H_z)_{\rm III}|_{\rho_2=\rho_{20}} = \sigma_{\rm g}(E_\phi)_{\rm II}|_{\rho_2=\rho_{20}}, \tag{23}$$
$$(H_\phi)_{\rm I}|_{\rho_1=\rho_{10}} - (H_\phi)_{\rm II}|_{\rho_1=\rho_{10}} = -\sigma_{\rm g}(E_z)_{\rm I}|_{\rho_1=\rho_{10}}, \tag{24}$$
$$(H_\phi)_{\rm II}|_{\rho_2=\rho_{20}} - (H_\phi)_{\rm III}|_{\rho_2=\rho_{20}} = -\sigma_{\rm g}(E_z)_{\rm II}|_{\rho_2=\rho_{20}}. \tag{25}$$

According to Eqs. (18)–(25), a set of linear algebraic equations can be obtained by using the point by point matching method[37] on the interface:

$$\begin{bmatrix} a_{mn}(0,0) & a_{mn}(0,1) & \cdots & a_{mn}(0,15)\\ a_{mn}(1,0) & a_{mn}(1,1) & \cdots & a_{mn}(1,15)\\ \cdots & \cdots & \cdots & \cdots\\ a_{mn}(7,0) & a_{mn}(7,0) & \cdots & a_{mn}(7,15)\end{bmatrix}\begin{bmatrix}[A]\\ [A']\\ \cdots\\ [H']\end{bmatrix} = 0. \tag{26}$$

Here, $[A]$ is a column vector composed of undetermined coefficients A_0, A_1, …, and A_m. $[A']$, …, and $[H']$, etc. $a_{mn}(i,j)$ is a submatrix of $m\times n$; for example,

$$a_{mn}(0,0) = I_m(\lambda_{11}\rho_{10})\cos(m\phi_{1n}). \tag{27}$$

The linear algebraic Eq. (26) is solved by our own Fortran 90 program. The distribution of field, the real part ${\rm Re}(n_{\rm eff})$ and the imaginary part ${\rm Im}(n_{\rm eff})$ of the effective refractive index of each mode can be obtained. The propagation length is given by the formula $L_{\rm prop} = \lambda/[4\pi{\rm Im}(n_{\rm eff})]$.[38,39] The figure of merit is given by ${\rm FoM} = {\rm Re}(n_{\rm eff})/{\rm Im}(n_{\rm eff})$,[39] which can be used to characterize the transmission performance of the waveguide.

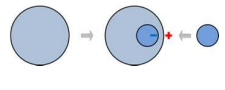
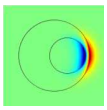
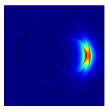
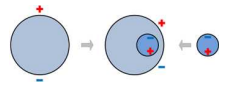
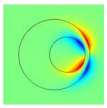
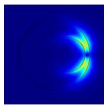
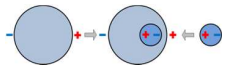
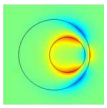
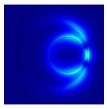
3. Results and discussion

3.1. Classification of modes

Table 1 shows the combination of the three lowest-order modes supported by the waveguide, the distribution of the electric field component in the z direction and the distribution of the electric field intensity under the conditions of $\lambda = 7$ μm, $E_{\rm f} = 0.5$ eV, $\rho_{10} = 75$ nm, $\rho_{20} = 150$ nm, $s = 20$ nm, $\varepsilon_1 = 1.0$, $\varepsilon_2 = 2.1025$, and $\varepsilon_3 = 1.0$. The three modes are named mode 0, mode 1 and mode 2 in turn. Mode 0 is combined by zero-order modes of the two single rods, and the electric field is mainly distributed in the gap region between the two layers of graphene on the right side of the waveguide. Mode 1 and mode 2 are combined by the first-order modes of two single

rods. The z component of the electric field of mode 1 is anti-symmetric about the horizontal axis, and the z component of the electric field of mode 2 is symmetric about the horizontal axis.

Table 1. The combination of the three lowest-order modes supported by the waveguide, the distribution of the electric field component in the z direction and the distribution of the electric field intensity under the conditions of $\lambda = 7$ μm, $E_f = 0.5$ eV, $\rho_{10} = 75$ nm, $\rho_{20} = 150$ nm, $s = 20$ nm, $\varepsilon_1 = 1.0$, $\varepsilon_2 = 2.1025$, and $\varepsilon_3 = 1.0$.

Mode name	Combination of modes	E_z	$\|E\|$
Mode 0			
Mode 1			
Mode 2			

3.2. Influence of working wavelength on transmission characteristics

Setting $E_f = 0.5$ eV, $\rho_{10} = 75$ nm, $\rho_{20} = 150$ nm, $s = 20$ nm, $\varepsilon_1 = 1.0$, $\varepsilon_2 = 2.1025$, and $\varepsilon_3 = 1.0$, the relationship between Re(n_{eff}), L_{prop}, and FoM of the three lowest-order modes and the working wavelength λ is shown in Figs. 2(a)–2(c). In these figures, the solid line is the result obtained using the FEM method, and the solid point line is the result obtained using the multipole method. If there is no special explanation, this marking method will be used in the following. With typical parameters, the conductivity of graphene varies greatly in the frequency range of 10 THz–100 THz, especially in the range of 40 THz–50 THz, and the corresponding wavelength range is about 6 μm–8 μm.[40] When the operating wavelength increases from 6.00 μm to 8.00 μm, the Re(n_{eff})-curves of the three lowest-order modes decrease monotonously and the distance between these curves increases. The L_{prop}-curves increase monotonically. The L_{prop}-curve of mode 2 intersects with the L_{prop}-curve of mode 0 at 7.00 μm, and intersects with the L_{prop}-curve of mode 1 at 7.00 μm. The FoM-curve corresponding to mode 0 increases gradually, and the FoM value of mode 1 and mode 2 reaches a peak at 7.0 μm and then decreases gradually. In the selected parameter range, mode 0 has the highest figure of merit and the best performance. The two embedded graphs in Fig. 2(b) show the field distribution of mode 0 when the operating wavelengths are 6.0 μm and 8.0 μm. Comparing the two embedded graphs, we can see that when the wavelength is short, the field distribution is mainly concentrated near the inner and outer graphene layers, and the electric field intensity is the largest near the inner graphene layer, and the interaction between the field and graphene is the largest. In addition, the waveguide loss is larger and the propagation length is shorter. When the wavelength is longer, the electric field diffuses to the dielectric layer between the two layers of graphene, the confinement of the waveguide to the field is weakened, the loss is reduced and the propagation length is longer.

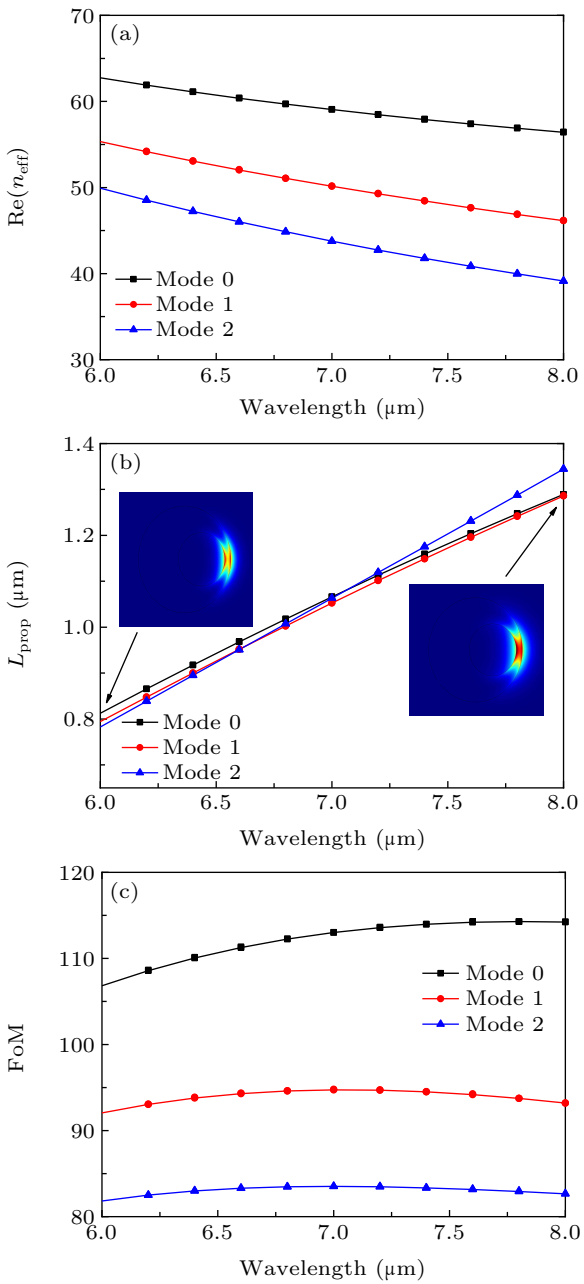


Fig. 2. The relationship between Re(n_{eff}), L_{prop}, and FoM of the three lowest-order modes and the working wavelength λ when $E_f = 0.5$ eV, $\rho_{10} = 75$ nm, $\rho_{20} = 150$ nm, $s = 20$ nm, $\varepsilon_1 = 1.0$, $\varepsilon_2 = 2.1025$, and $\varepsilon_3 = 1.0$.

3.3. Influence of the radius of wire 1 on transmission characteristics

Setting $\lambda = 7$ μm, $E_f = 0.5$ eV, $\rho_{20} = 150$ nm, $s = 20$ nm, $\varepsilon_1 = 1.0$, $\varepsilon_2 = 2.1025$, and $\varepsilon_3 = 1.0$, the relationship between Re(n_{eff}), L_{prop} and FoM of the three lowest-order modes and the radius ρ_{10} of wire 1 is shown in Figs. 3(a)–3(c). As the radius of the inner wire ρ_{10} increases gradually, the real part

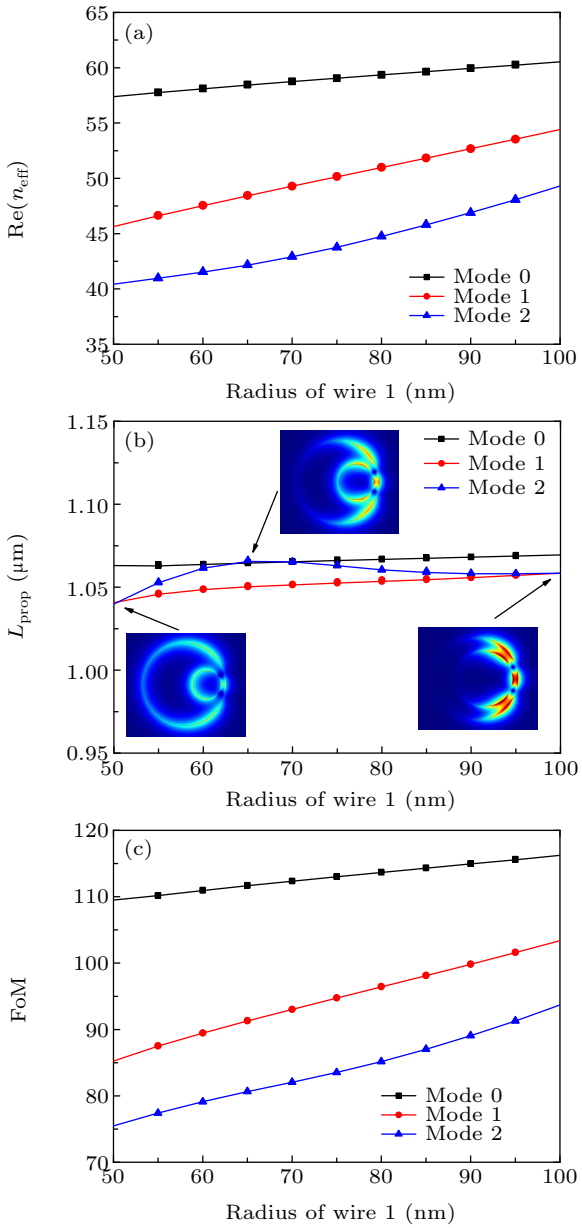


Fig. 3. The relationship between Re($n_{\rm eff}$), $L_{\rm prop}$, and FoM of the three lowest-order modes and the radius ρ_{10} of wire 1 when $\lambda = 7.0$ μm, $E_{\rm f} = 0.5$ eV, $\rho_{20} = 150$ nm, $s = 20$ nm, $\varepsilon_1 = 1.0$, $\varepsilon_2 = 2.1025$, and $\varepsilon_3 = 1.0$.

of the effective refractive index Re($n_{\rm eff}$) of mode 0, mode 1 and mode 2 increase monotonically. The $L_{\rm prop}$ of mode 0 and mode 1 increase slowly and monotonically, while the $L_{\rm prop}$ of mode 2 increases gradually at first, reaches maximum at 65 nm, and then decreases gradually. In the selected parameter range, mode 0 has the highest figure of merit and the best performance. The three embedded graphs in Fig. 3(b) show the field distribution of mode 2 when the radius of the inner wire ρ_{10} is 50 nm, 65 nm, and 100 nm. Comparing the three embedded graphs, we can see that when $\rho_{10} = 50$ nm, the field is widely distributed on the inner and outer graphene layers, and the interaction between the field and graphene is large. In addition, the waveguide loss is large and the propagation length is short. When ρ_{10} increases gradually, the field shifts to the right side of the waveguide and gradually concentrates to the region between the two layers of graphene. When $\rho_{10} = 65$ nm, the field distribution decreases, the field intensity is not very strong and the interaction between the field and graphene is the smallest. Furthermore, the waveguide loss is the smallest and the propagation length is the longest. When $\rho_{10} = 100$ nm, the field is mainly concentrated between the inner and outer graphene layers on the right side of the waveguide. The field intensity is higher and the interaction between the field and graphene becomes larger. In addition, the waveguide loss becomes larger and the propagation length becomes shorter.

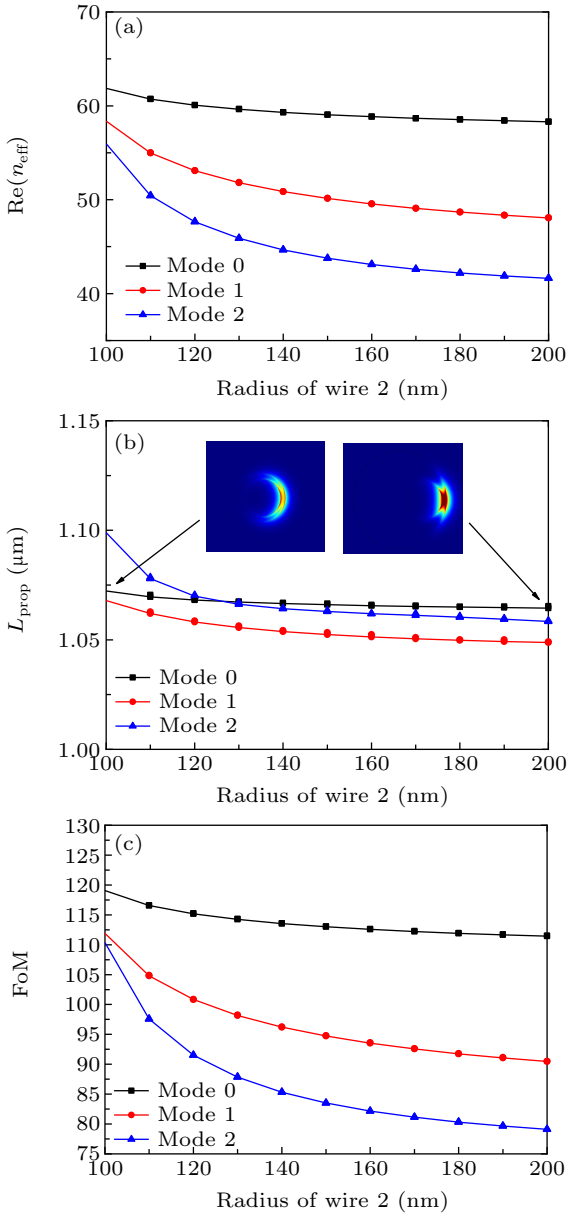


Fig. 4. The dependence of Re($n_{\rm eff}$), $L_{\rm prop}$, and FoM of the three lowest-order modes on the radius ρ_{20} of wire 2 when $\lambda = 7.0$ μm, $E_{\rm f} = 0.5$ eV, $\rho_{10} = 75$ nm, $s = 20$ nm, $\varepsilon_1 = 1.0$, $\varepsilon_2 = 2.1025$, and $\varepsilon_3 = 1.0$.

3.4. Influence of the radius of wire 2 on transmission characteristics

Setting $\lambda = 7$ μm, $E_{\rm f} = 0.5$ eV, $\rho_{10} = 75$ nm, $s = 20$ nm, $\varepsilon_1 = 1.0$, $\varepsilon_2 = 2.1025$, and $\varepsilon_3 = 1.0$, the dependence of

Re(n_{eff}), L_{prop}, and FoM of the three lowest-order modes on the radius ρ_{20} of wire 2 is shown in Figs. 4(a)–4(c). When the radius ρ_{20} of the outer wire is increased, the real part of the effective index of mode 0, mode 1 and mode 2 monotonically decreases, and the distance between the curves increases. The propagation length of the three modes decreases slowly, but the change is not significant. In the selected parameter range, mode 0 has the highest figure of merit and the best performance. The two images embedded in Fig. 4(b) show the field distribution map corresponding to mode 0 when ρ_{20} is 100 nm and 200 nm, respectively. Comparing the two embedded images, we can see that the field is concentrated in the area near the inner and outer graphene layers on the right side of the waveguide. When $\rho_{20} = 100$ nm, the distribution range of the field is large, but the intensity of the field is weak. When $\rho_{20} = 200$ nm, the distribution range of the field is small, but the intensity of the field is strong. In both cases, the interaction strength between the field and graphene is close, the waveguide loss is close and the propagation length is also close.

3.5. Influence of the minimum spacing on transmission characteristics

Setting $\lambda = 7$ μm, $E_{\text{f}} = 0.5$ eV, $\rho_{10} = 75$ nm, $\rho_{20} = 150$ nm, $\varepsilon_1 = 1.0$, $\varepsilon_2 = 2.1025$, and $\varepsilon_3 = 1.0$, the dependence of Re(n_{eff}), L_{prop}, and FoM of the three lowest-order modes on the minimum spacing between the inner and outer cylinders s are shown in Figs. 5(a)–5(c). Increasing the minimum spacing between the inner and outer cylinders, the real part of the effective index of the three modes monotonically decreases, and the spacing between the curves becomes smaller. The propagation lengths of the three modes increase monotonously, the curve corresponding to mode 0 increases faster than that corresponding to mode 1, and the curve corresponding to mode 2 intersects with the other two curves. The transmission performance of mode 0 and mode 1 decreases, while the transmission performance of mode 2 is almost unaffected. The two embedded images in Fig. 5(b) show that the field distribution of mode 0 corresponding to s is 10 nm and 30 nm, respectively. Comparing the two embedded images, we can see that when the minimum spacing between the inner and outer cylinders is small, the area of field distribution is small, the field intensity is high, the confinement of the waveguide to the field is strong, the interaction between the field and graphene is strong, the waveguide loss is large and the propagation length is short. When the minimum spacing between the inner and outer cylinders is large, the area of field distribution is large, the field strength is weak, the confinement of the waveguide to the field is weak, the interaction between the field and graphene is weak, the waveguide loss is small and the propagation length is long.

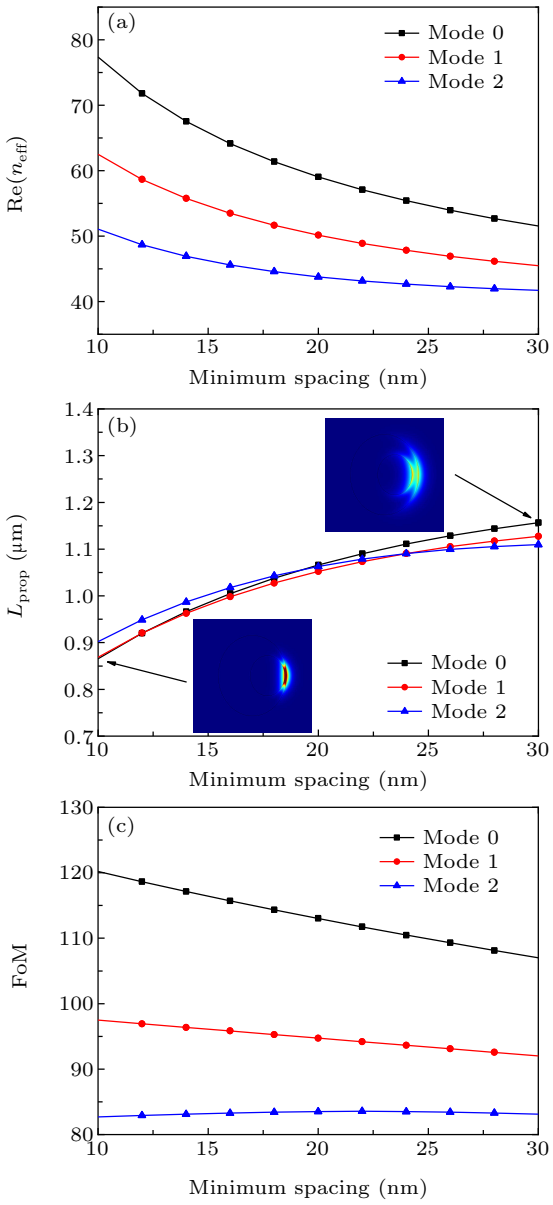


Fig. 5. The dependence of Re(n_{eff}), L_{prop}, and FoM of the three lowest-order modes on the minimum spacing between the inner and outer cylinders s when $\lambda = 7.0$, $E_{\text{f}} = 0.5$ eV, $\rho_{10} = 75$ nm, $\rho_{20} = 150$ nm, $\varepsilon_1 = 1.0$, $\varepsilon_2 = 2.1025$ and $\varepsilon_3 = 1.0$.

3.6. Influence of the Fermi energy on transmission characteristics

Setting $\lambda = 7$ μm, $\rho_{10} = 75$ nm, $\rho_{20} = 150$ nm, $s = 20$ nm, $\varepsilon_1 = 1.0$, $\varepsilon_2 = 2.1025$, and $\varepsilon_3 = 1.0$, the dependence of Re(n_{eff}), L_{prop}, and FoM of the three lowest-order modes on the Fermi energy E_{f} is shown in Figs. 6(a)–6(c). With the increase in E_{f}, the real part of the effective refractive index of the three lowest-order modes decreases monotonously, the confinement of the waveguide to the field decreases, the interaction between the field and graphene weakens, the loss decreases and the propagation length increases. In this changing process, the propagation length of the three modes shows little difference. When the Fermi energy of graphene increases from 0.2 eV

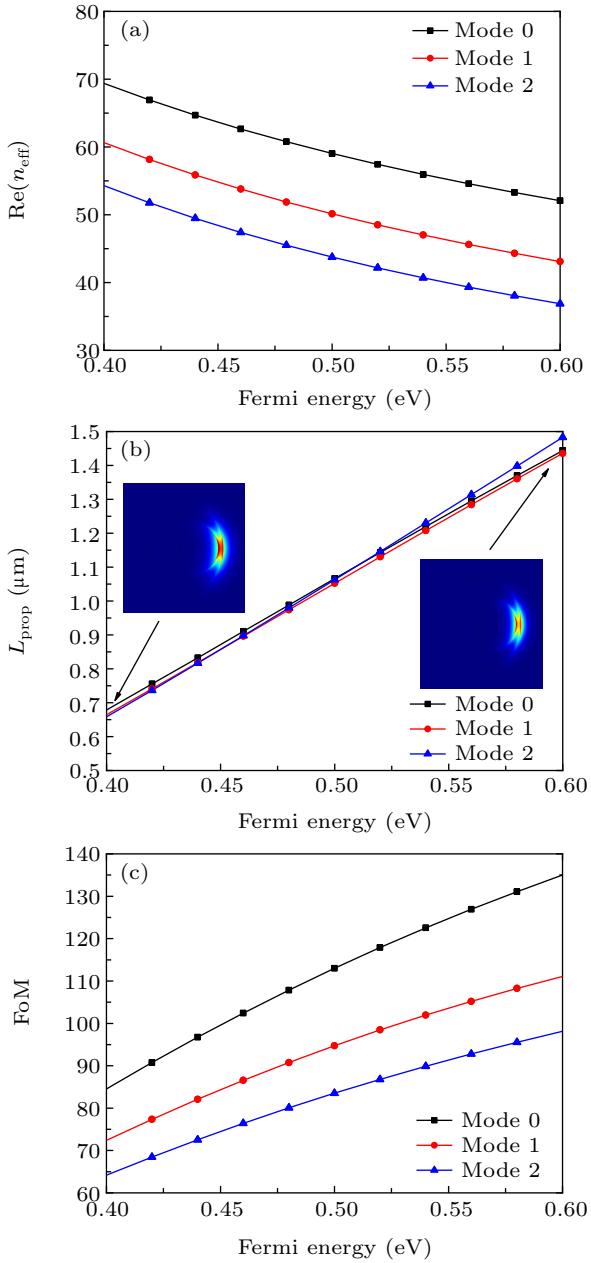


Fig. 6. The dependence of Re($n_{\rm eff}$), $L_{\rm prop}$, and FoM of the three lowestorder modes on the Fermi energy $E_{\rm f}$ when $\lambda = 7.0$ μm, $\rho_{10} = 75$ nm, $\rho_{20} = 150$ nm, $s = 20$ nm, $\varepsilon_1 = 1.0$, $\varepsilon_2 = 2.1025$, and $\varepsilon_3 = 1.0$.

to 0.8 eV, the propagation length of mode 2 will gradually exceed the other two modes. Mode 0 always leads the other two modes with a higher figure of merit. By adjusting the Fermi level of graphene, the mode transmission performance can be improved obviously. The two embedded images in Fig. 6(b) show the field distribution of mode 0 when $E_{\rm f}$ is 0.2 eV and 0.8 eV, respectively. Comparing the two embedded images, we can see that when the Fermi energy of graphene is small, the field distribution is mainly confined to the inner and outer graphene layers, the intensity of the field on the graphene is high, the confinement of the waveguide to the field is strong, the interaction between the field and graphene is strong, the waveguide loss is large and the propagation length is short. When the Fermi energy of graphene is large, the field diffuses to the dielectric layer between the two layers of graphene, the field strength on the graphene is weak, the confinement of the waveguide to the field is weak, the interaction between the field and graphene is weak, the waveguide loss is small and the propagation length is long.

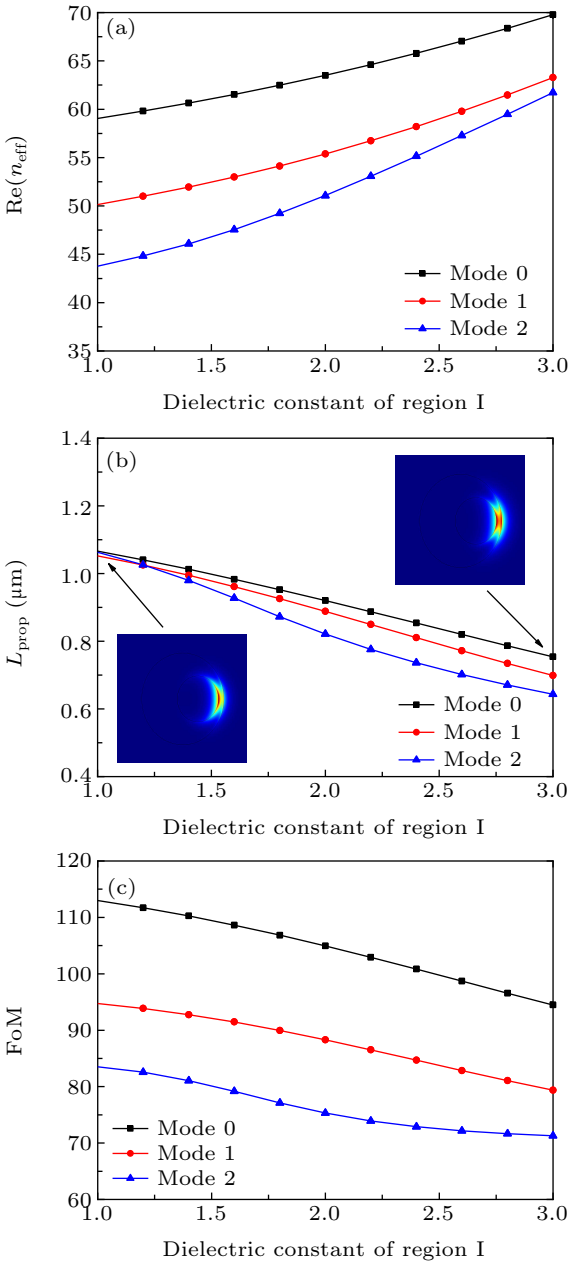


Fig. 7. The dependence of Re($n_{\rm eff}$), $L_{\rm prop}$ and FoM of the three lowestorder modes on the dielectric constant of region I ε_1 when $\lambda = 7.0$ μm, $E_{\rm f} = 0.5$ eV, $\rho_{10} = 75$ nm, $\rho_{20} = 150$ nm, $s = 20$ nm, $\varepsilon_2 = 2.1025$, and $\varepsilon_3 = 1.0$.

3.7. Influence of the dielectric constant of region I on transmission characteristics

Setting $\lambda = 7$ μm, $E_{\rm f} = 0.5$ eV, $\rho_{10} = 75$ nm, $\rho_{20} = 150$ nm, $s = 20$ nm, $\varepsilon_2 = 2.1025$, and $\varepsilon_3 = 1.0$, the dependence of Re($n_{\rm eff}$), $L_{\rm prop}$, and FoM of the three lowest-order modes on the dielectric constant of region I ε_1 is shown in Figs. 7(a)–7(c). With the increase in ε_1, the real parts of the effective refractive index of the three lowest-order modes in-

crease monotonically, the confinement of the waveguide to the field becomes stronger, the interaction between the field and graphene becomes stronger, the loss increases, the propagation length decreases monotonously and the quality factor of the mode decreases gradually. The two embedded images in Fig. 7(b) show the field distribution of mode 0 when ε_1 is 1.0 and 3.0, respectively. Comparing the two embedded images, we can see that when the dielectric constant of region I is small, the field intensity, the confinement of the waveguide to the field and the interaction between the field and graphene are weak. In addition, the waveguide loss is small and the propagation length is long. In contrast, when the dielectric constant of region I is large, the field intensity, the confinement of the waveguide to the field and the interaction between the field and graphene are strong, the waveguide loss is large and the propagation length is short.

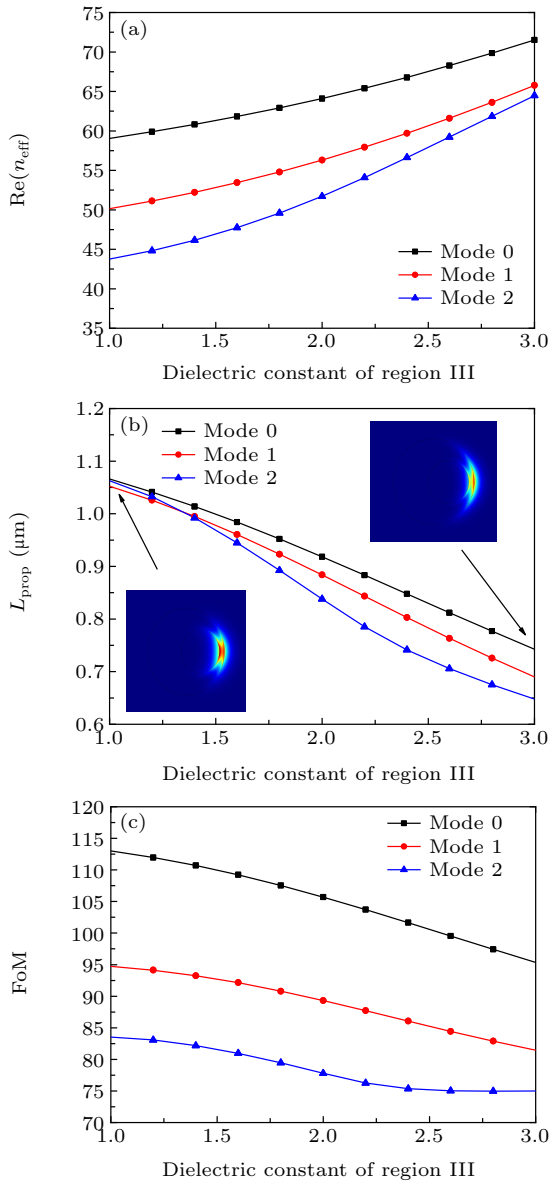


Fig. 8. The dependence of Re($n_{\rm eff}$), $L_{\rm prop}$, and FoM of the three lowest-order modes on the dielectric constant of region III ε_3 when $\lambda = 7.0$ μm, $E_{\rm f} = 0.5$ eV, $\rho_{10} = 75$ nm, $\rho_{20} = 150$ nm, $s = 20$ nm, $\varepsilon_1 = 1.0$, and $\varepsilon_2 = 2.1025$.

3.8. Influence of the dielectric constant of region III on transmission characteristics

Setting $\lambda = 7$ μm, $E_{\rm f} = 0.5$ eV, $\rho_{10} = 75$ nm, $\rho_{20} = 150$ nm, $s = 20$ nm, $\varepsilon_1 = 1.0$, and $\varepsilon_2 = 2.1025$, the dependence of Re($n_{\rm eff}$), $L_{\rm prop}$, and FoM of the three lowest-order modes on the dielectric constant of region III ε_3 is shown in Figs. 8(a)–8(c). Increasing ε_3, the real parts of the effective refractive index of the three lowest-order modes increase monotonically, and the confinement of the waveguide to the field becomes stronger. The interaction between the field and graphene becomes stronger, the loss increases, the propagation length decreases monotonously, and the figure of merit of the mode decreases gradually. The two embedded images in Fig. 8(b) show the field distribution of mode 0 when ε_3 is 1.0 and 3.0, respectively. Comparing the two embedded images, we can see that when the dielectric constant of region III is small, the intensity of the field is weak, the confinement of the waveguide to the field is weak, the interaction between the field and graphene is weak, the waveguide loss is small and the propagation length is long. When the permittivity of region III is large, the field intensity is strong, the confinement of the waveguide to the field is strong, the interaction between the field and graphene is strong, the waveguide loss is large and the propagation length is short.

4. Conclusion

The multipole method can effectively solve the mode problem of the graphene coated nested dielectric waveguide. Mode 0 is combined by the zero-order modes of two single nanowires. Mode 1 and mode 2 are combined by the first-order modes of two single nanowires. Within the selected parameter range, we find that mode 0 has the highest quality factor and the best performance. As the wavelength, the minimum spacing between the inner and the outer cylinders, the radius of the inner cylinder and the Fermi energy of graphene increase, the confinement of the waveguide to the three lowest-order modes decreases, the loss decreases and the propagation length increases. When the radius of the outer cylinder, the dielectric constant of region I or the dielectric constant of region III increases, the confinement of the waveguide to the three lowest-order modes increases, the loss increases and the propagation length decreases. These results have been verified by the FEM method. This work has provided a theoretical basis for the design, fabrication and application of nested dielectric nanowire waveguides coated with graphene.

Acknowledgments

Project supported by the Natural Science Foundation of Shanxi Province, China (Grant Nos. 201901D111159 and

2021D20021310) and the Shanxi Scholarship Council of China (Grant No. HGKY2019068).

References

[1] Barnes W L, Dereux A and Ebbesen T W 2003 *Nature* **424** 824
[2] Bozhevolnyi S I, Volkov V S, Devaux E, *et al.* 2006 *Nature* **440** 508
[3] Oulton R F, Sorger V J, Genov D A, *et al.* 2008 *Nat. Photon.* **2** 496
[4] Vakil A and Engheta N 2011 *Science* **332** 1291
[5] MacDonald K F and Zheludev N I 2010 *Laser Photon. Rev.* **4** 562
[6] Cheng Y, Yang J, Lu Q, *et al.* 2016 *Sensors* **16** 773
[7] Wang J, Wang X, Shao H, *et al.* 2017 *Nanoscale Res. Lett.* **12** 9
[8] Bao Z, Wang J, Hu Z D, *et al.* 2019 *Opt. Express* **27** 31435
[9] Chen Y, Pan X, Bao Z, *et al.* 2021 *IEEE Photon. J.* **13** 4800312
[10] Christensen J, Manjavacas A, Thongrattanasiri S, *et al.* 2012 *ACS Nano* **6** 431
[11] Gao Y, Ren G, Zhu B, J. *et al.* 2014 *Opt. Lett.* **39** 5909
[12] Gao Y, Ren G, Zhu B, *et al.* 2014 *Opt. Express* **22** 24322
[13] Yang J, Yang J, Deng W, *et al.* 2015 *Opt. Express* **23** 32289
[14] Liu J P, Zhai X, Xie F, *et al.* 2017 *J. Lightwave Technol.* **35** 1971
[15] Xing R and Jian S 2017 *IEEE Photon. Technol. Lett.* **29** 967
[16] Nikitin A Y, Guinea F, Garcia-Vidal F J, *et al.* 2011 *Phys. Rev. B* **84** 161407
[17] Kim J T and Choi S Y 2011 *Opt. Express* **19** 24557
[18] He S, Zhang X and He Y 2013 *Opt. Express* **21** 30664
[19] Cheng X, Xue W R, Wei Z N, *et al.* 2019 *Opt. Commun.* **452** 467
[20] Liu P, Zhang X, Ma Z, *et al.* 2013 *Opt. Express* **21** 32432
[21] Xu W, Zhu Z H, Liu K, *et al.* 2015 *Opt. Express* **23** 5147
[22] Gosciniak J and Tan D T H 2013 *Nanotechnology* **24** 185202
[23] Sun Y, Zheng Z, Cheng J, *et al.* 2014 *Opt. Commun.* **328** 124
[24] Lin I T and Liu J M 2014 *Appl. Phys. Lett.* **105** 011604
[25] Xing R and Jian S 2017 *IEEE Photon. Technol. Lett.* **29** 1643
[26] Huang Y, Zhang L, Yin H, *et al.* 2017 *Opt. Lett.* **42** 2078
[27] Zhu B, Ren G, Yang Y, *et al.* 2015 *Plasmonics* **10** 839
[28] Xing R and Jian S 2016 *IEEE Photon. Technol. Lett.* **28** 2779
[29] Ye S, Wang Z, Sun C, *et al.* 2018 *Opt. Express* **26** 23854
[30] Wijngaard W 1973 *J. Opt. Soc. Am.* **63** 944
[31] Nikitin A Y, Guinea F, Garcia-Vidal F J, *et al.* 2011 *Phys. Rev. B* **84** 195446
[32] Yuan T, Zhang X, Xia Q, *et al.* 2021 *J. Lightwave Technol.* **39** 290
[33] Chen K, Zhou X, Cheng X, *et al.* 2019 *Nat. Photon.* **13** 754
[34] Yeh C and Shimabukuro F I 2008 *The Essence of Dielectric Waveguides* (Springer Science + Business Media, New York) p. 41
[35] Lee W M 2011 *J. Sound Vib.* **330** 4915
[36] Lee W M 2014 *International Journal of Mechanical Sciences* **78** 203
[37] Erricolo D and Carluccio G 2013 *ACM Trans. Mathematical Software* **40** 1
[38] He X, Ning T, Lu S, *et al.* 2018 *Opt. Express* **26** 10109
[39] Hajati M and Hajati Y 2018 *Plasmonics* **13** 403
[40] Sensale-Rodriguez B 2015 *J. Lightwave Technol.* **33** 1100